1   **Slowdown of Shirase Glacier caused by strengthening alongshore winds**

3   Bertie W.J. Miles*[1,2], Chris R. Stokes[2], Adrian Jenkins[3], Jim .R. Jordan[3,4], Stewart .S.R. Jamieson[2],

4   G. Hilmar. Gudmundsson[3]

6   [1]School of Geosciences, Edinburgh University, Edinburgh, EH8 9XP, UK

7   [2]Department of Geography, Durham University, Durham, DH1 3LE, UK

8   [3]Department of Geography and Environmental Sciences, Northumbria University, Newcastle upon

9   Tyne, NE1 8ST, UK

10   [4]Laboratoire de Glaciologie, Université Libre de Bruxelles, Brussels, Belgium

11   *Correspondence to Bertie.Miles@ed.ac.uk

13   **Abstract**

14   Observations have confirmed basal melt rates of up to 16 m a^{-1} underneath the Shirase ice tongue in

15   East Antarctica. These high basal melt rates are caused by intrusions of warm modified Circumpolar

16   Deep Water (mCDW) onto the continental shelf, a mechanism responsible for widespread mass loss

17   in West Antarctica, together with parts of Wilkes Land. In contrast to those regions, the catchment of

18   Shirase Glacier has been gaining mass, a trend attributed to increased precipitation. Here, we report

19   on the dynamical ocean-driven slowdown, thickening and grounding line advance of Shirase Glacier,

20   in response to strengthening easterly winds that reduce mCDW inflow and decrease basal melt rates.

21   Our findings are significant because they demonstrate that warm water regimes are not universally

22   associated with glacier acceleration and mass loss in Antarctica, and they highlight the overlooked

23   role of ocean forcing in the recent mass gain of the Dronning Maud Land sector.

24

25   **1. Introduction**

26   Shirase Glacier is the fastest flowing outlet glacier in East Antarctica, reaching speeds in excess of

27   2,200 m a^{-1} across its grounding line, before flowing into Lützow-Holm Bay (Fig. 1). Its annual ice

28   discharge approaches 15 Gt a^{-1} (Rignot et al., 2019) and it drains a catchment containing 1.2 m of sea

29   level equivalent (Fig.1, Morlighem et al., 2020). This rapid ice flow speed is associated with vigorous

30   melt underneath its floating tongue, where basal melt rates have been observed to vary seasonally
31   between 7 and 16 m a^{-1} in 2018, 16 km downstream of the glacier's grounding line (Hirano et al.,
32   2020). These high melt rates are caused by warm modified Circumpolar Deep Water (mCDW)
33   intruding onto the continental shelf and being transported directly to the glacier via bathymetric
34   troughs (Fig. 1; Moriwaki & Yoshida, 1983; Hirano et al., 2020), a process referred to as Mode 2
35   melting (Jacobs et al., 1992). Elsewhere in Antarctica, most regions that experience this mode of
36   oceanic melt have been losing mass, as enhanced melt has thinned ice shelves, causing glacier
37   acceleration and mass loss e.g. the Amundsen Sea (Jenkins et al., 2018; Mouginot et al., 2014), the
38   Western Antarctic Peninsula (Cook et al., 2016) and Wilkes Land (Rintoul et al., 2016; Greene et al.,
39   2017). However, mass loss has not been observed at Shirase Glacier and, between 2003 and 2019, its
40   wider catchment (sometimes referred to as drainage basin 7) gained mass at a rate of +25 ± 6 Gt a^{-1},
41   which is the largest imbalance of all drainage basins in East Antarctica (Smith et al., 2020), including
42   the comparatively well studied Wilkes Land (drainage basin 13; -20 ± 14 Gt a^{-1}).

43   The mass gain and thickening in the Shirase catchment over the past two decades has been
44   hypothesized to have been caused by increased precipitation (Schröder et al., 2019; Smith et al., 2020)
45   from extreme snowfall events within the wider region (Boening et al., 2012; Lenaerts et al., 2013).
46   Although, earlier field-based estimates, using repeat triangulation surveys in 1969 and 1973,
47   demonstrated ice surface lowering of around 0.7 m a^{-1} around 100-200 km inland of the Shirase
48   Glacier grounding line (Mae & Naruse, 1978; Naruse, 1979; Nishio et al., 1989). Furthermore, repeat
49   GPS surveys in 1980 and 1988 revealed a thinning rate of around 0.5 m a^{-1} 100-150 km inland of the
50   grounding line (Toh et al., 1992). These rates of surface lowering during that time are comparable
51   with some of the fastest rates of thinning observed across Antarctica over the past decade at similar
52   distances inland of the grounding line (Smith et al., 2020). This surface lowering may have a much
53   longer-term signal with ice core records estimating a surface lowering of 350 m over the past 2000
54   years of the Mizuho Plateau (Kameda et al., 1990), which is located around 200 km inland of the
55   Shirase coastline. The surface lowering over the past 2000 years is coincident with an increase in ice
56   discharge from the Lützow-Holm Bay, which has been estimated from subglacial erosion rates
57   (Sproson et al., 2021).

58   Oceanographic observations in Lützow-Holm Bay in 2018 have revealed a two-layered structure with
59   a cool and relatively fresh layer of Winter Water overlying a warm and saline mCDW layer, where
60   temperatures near the ice front seasonally exceed the *in situ* melting point by 2.7 °C (Hirano et al.,
61   2020). Observations and modelling demonstrate a strong seasonal variation in the basal melt rate of
62   the Shirase ice tongue (Hirano et al., 2020; Kusahara et al., 2021), which is caused by seasonal
63   variations in the depth of the thermocline forced by the strength of the alongshore easterly winds near

64   the continental shelf (Ohshima et al., 1996). There is no evidence of large seasonal variations in ice

65   flow speed at the grounding line, but observations do show some seasonal variation in ice flow speed

66   on the floating tongue that could be connected to external forcing (Nakamura et al., 2007; 2010).

67   There have been several studies analysing the ice flow dynamics of the Shirase Glacier, largely

68   covering short sub-decadal time periods (Pattyn & Derauw, 2002; Pattyn & Naruse, 2003; Nakamura

69   et al., 2010; Aoyama et al., 2013). However, the longer-term geological signal of ice sheet thinning

70   and increased ice discharge, along with observations of thinning in the 1970s and 1980s, followed by

71   thickening from the 2000s raise some important questions into the processes causing this switch. In

72   this study, we produce a time series of ice flow speed that spans 47 years and show that long-term ice

73   speed trends coincide with alongshore wind speeds. We then discuss how these observations may

74   relate to wider hemispheric trends in atmospheric circulation and what this may mean for the future

75   mass balance of the Shirase catchment and the wider Dronning Maud Land sector.
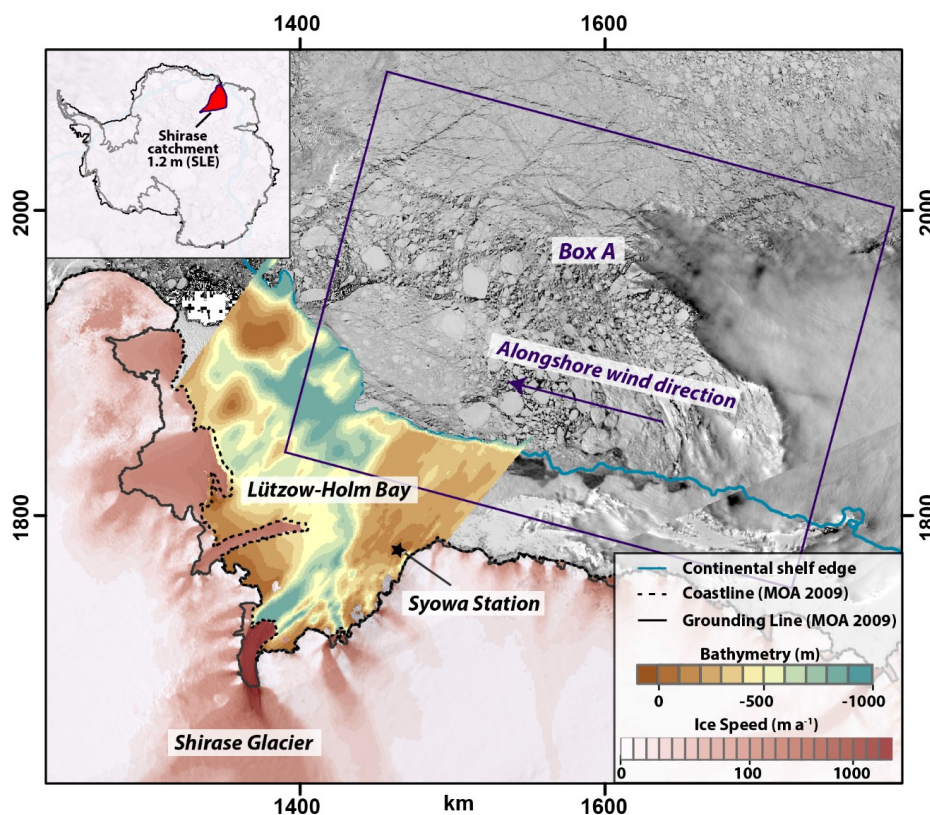
76

77   **Figure 1:** MODIS image of Lützow-Holm Bay and Shirase Glacier from the 4th November 2019
78   obtained from NASA WorldView. Overlain is the ITS_LIVE composite velocity product in
79   logarithmic scale (Gardner et al., 2018; 2020), the MODIS 2009 grounding line and coastline (black
80   line; Scambos et al., 2007; Harran et al., 2019), 1000 m bathymetric contour obtained from

81   BedMachine (Morlighem et al., 2020) which is taken as the continental shelf boundary and
82   bathymetry of the Lützow-Holm Bay (Kusahara et al., 2021). Note the deep trough connecting Shirase
83   Glacier to the open ocean. The location of the Syowa research station and Box A, the region where
84   ERA5 derived winds were extracted are also shown. The coordinate grid is in km and it is projected
85   in Polar Stereographic.

86

2. Data and Methods

2.1 Ice-front position, ice speed, grounding line and ice thickness

89   We create a time series of ice-front positions between 1963 and 2020 using a variety of different

90   sources including: ARGON imagery from 1963, Landsat-1 imagery from 1973, Landsat-5 imagery

91   from 1984, Landsat-4 imagery from 1988, RADARSAT RAMP mosaic from 1997 (Jezek et al.,

92   2013), and MODIS imagery from 2000-2020, with the spatial resolution of the satellite data ranging

93   from 15-250 m. In each case, we map the outer limit of the collection of loosely bound icebergs that

94   form the Shirase ice tongue that are typically surrounded by a smoother surface of fast ice (Fig. 1 &

95   2a). Errors associated with this mapping are insignificant in the context of the ice tongue typically

96   advancing 2,500 m a^{-1}, or retreating in short-lived calving events typically >10 km.

97   We calculate 18 ice speed estimates for Shirase Glacier between 1973 and 2020. For 1973 we use a

98   pair of Landsat-1 (band 7) images from the 25th January 1973 and the 21st January 1974 that we

99   manually co-register to each other, before co-registering to a Landsat-8 image. The combination of

100   the relatively coarse Landsat-1 imagery (60 m) and the development of surface melt ponding over the

101   fast flowing section of the glaciers between the two images prevented the automatic extraction of ice

102   speed. Instead, we extract an ice speed estimate by manually tracking the displacement of a prominent

103   rift ~24 km downstream of the grounding line (Fig. 2c). Errors associated with the manual tracking

104   of this rift stem from the co-registration between the two image pairs which we estimate to be one

105   pixel (60 m; Animation S1). For 1988, we use a pair of Landsat-4 (band 3) images from the 14th

106   January 1988 and the 15th February 1988 that we also co-register to a Landsat-8 image. The quality

107   of the Landsat-5 images (30 m resolution) is superior to that of the Landsat-1 imagery and, in the

108   absence of significant surface melt ponding, we use the feature tracking software COSI-CORR

109   (Leprince et al., 2007; Scherler et al., 2008) to extract ice speed. For these images co-registration

110   error is negligible (Animation S2) and error in the feature tracking is estimated at <0.5 pixels (e.g.

111   Heid and Kääb, 2012), because of the close time separation of the image pairs this results in a larger

112   error of ±171 m a^{-1}. For 2000-2018 we use 14 annual ice speed mosaics from the ITS_LIVE dataset

113   which cover Shirase Glacier (Gardner et al., 2018) and use the corresponding error grids for error

114   values, which range from 1 to 32 m a^{-1}. For 2019 (n=27) and 2020 (n=19) we take an average for all

115 GoLIVE generated ice speed fields (Fahnestock et al., 2016; Scambos et al., 2016) with a time

116 separation of 16-320 days from scene ID's 149_109 and 150_109. Taking an average of multiple ice

117 speed grids reduces error and, as such, we prescribe a nominal error of 16 m a^{-1}. We extract ice speed

118 profiles from each time period across a transect, T1 (Fig. 2a), and also produce a time-series of ice

119 speed change where T1 crosses the grounding line. In 1973, the only possible observation of ice speed

120 was extracted 24 km downstream of the grounding line (Point x; Fig. 2a) and there are no observations

121 directly at the grounding line. To account for this, we estimate ice speed at the grounding line in 1973

122 using the average difference between point x, 24 km downstream of the grounding line, and where

123 T1 crosses the grounding line in each of the other 17 ice speed profiles (1988-2020). Across these

124 profiles, ice speed was on average 2% slower (ranging from 1% to 4%) at the grounding line,

125 compared to ice speed at point x. Therefore, to estimate ice speed at the grounding line in 1973 we

126 reduce the ice speed observed 24 km downstream of the grounding line by 2 ±1%. We also include

127 the measurements of ice speed from Nakamura et al. (2007) at the grounding line derived from the

128 JERS-1 satellite in 1996, 1997 and 1998.

129 To estimate the direction and magnitude of any migration in the Shirase Glacier grounding line we

130 compare time stamped digital elevation model (DEM) strips with a spatial resolution of 2 m from the

131 6th January 2013 and the 8th October 2015 from the REMA project (Howat et al., 2019). We select

132 these strips because they cover the complete Shirase Glacier grounding line and represent the longest

133 time gap in the record. This is in addition to a SPOT5-HRS DEM from the SPIRIT project (Korona

134 et al., 2009) from the 8th February 2008, with a spatial resolution of 40 m. Elevation uncertainty is

135 estimated at around 4 m by comparing derived elevations from exposed bedrock between the two

136 REMA DEM's and a larger uncertainty of around 7 m between the SPOT5-HRS and REMA DEM's.

137 The tidal amplitude of the region is limited to 0.2 m (Aoki et al., 2000) and is deemed insignificant.

138 We extract elevation profiles along transect T1 (Fig. 2a) from these dates. A comparison of elevation

139 profiles cannot provide a location of the true grounding line position, but any horizontal migration of

140 these elevation slopes can provide reasonable estimates in both the direction and rate of grounding

141 line migration (Fricker et al., 2009; Brunt et al., 2010).

142 We also extract an ice thickness change time-series from the dataset presented in Schröder et al.

143 (2019) from point IT, which is around 20 km inland of the grounding line (Fig. 2a). This multi-

144 mission dataset spans between 1978 and 2017 and contains data from a variety of satellites. We use

145 the accompanying uncertainty estimates described in Schröder et al. (2019). We also utilize modelled

146 melt rate anomalies of the Shirase ice tongue that are derived by an ocean model that is forced by

147 ERA5 wind reanalysis between 2008 and 2018 by Kusahara et al. (2021). The melt rate dataset

148 contains melt anomalies that have been simulated with and without fast ice cover, we use the melt

149 rates with fast ice cover, but note that there is little difference between the two melt rate datasets (see

150 Fig. 20; Kusahara et al., 2021)

151

152 **2.2 Climatological data**

153 We extract mean monthly ERA5 (Hersbach et al., 2020) 10 m zonal (U) and meridional winds (V)

154 speeds with a gridded 30 km spatial resolution between 1979 and 2020 from an approximately 340 x

155 250 km box adjacent to the coastline (Box A; Fig. 1). We do not extend the box all the way into

156 Lützow-Holm Bay because it is semi-permanently covered with landfast sea-ice (Fig. S1) that

157 dampens the impact of winds on ocean circulation. We also utilize an observational wind direction

158 and wind speed time-series (1966-2020) from the Syowa research station (See Fig.1) that is available

159 via the SCAR Met READER (Turner et al., 2004). We then calculate alongshore easterly wind speed

160 for both the ERA5 reanalysis data extracted from Box A and the observational time-series from

161 Syowa research station, using an alongshore angle of 80° from due north:

162 $$A = W \cos(\theta - 80)$$

163 Where W is wind speed and θ is wind direction. Some   differences   between   the   ERA5   and

164 observational record from Syowa are expected because the ERA5 record represents an average from

165 a much larger region, while the observational data from Syowa research station are from a single

166 spatial location.

167

168 **3. Results**

169 We observe a total range of nearly 90 km in the ice-front position of the Shirase ice tongue between

170 1963 and 2020. Its maximum extent was in 1963, before retreating to its minimum extent in 1988

171 (Fig. 2a, b). Since 1988 there has been a general pattern of advance with a few sporadic calving events

172 (Fig. 2a, b). Most of the variation in the extent of the Shirase ice tongue is in the heavily fractured

173 and unconstrained section of the floating ice tongue. The only exception to this was in 1988 when the

174 ice tongue retreated to the entrance of the narrow and more constrained section of its fjord, 24 km

175 advanced of its 2009 grounding line (Fig. 2a).
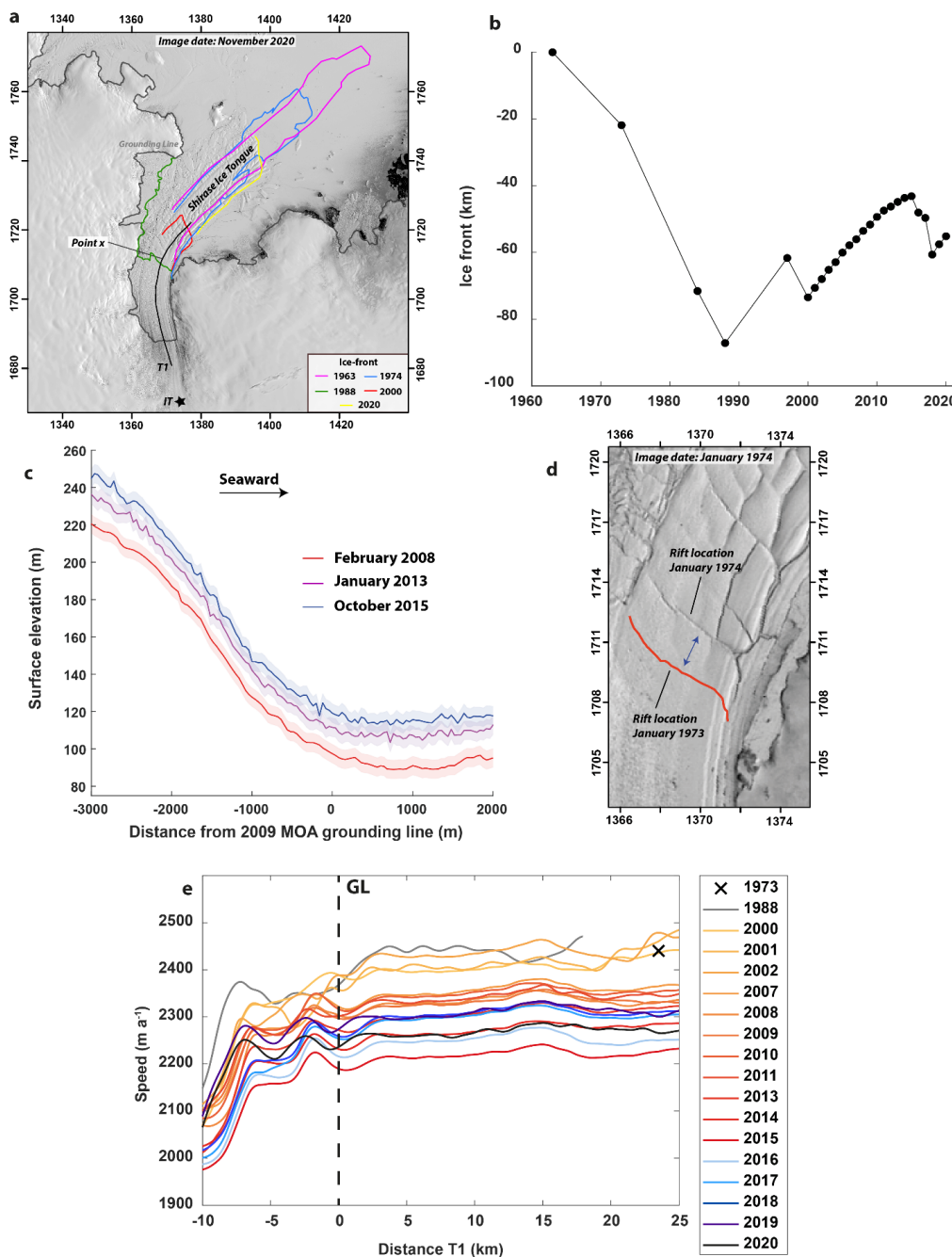
Figure 2: a) Landsat-8 image from November 2020 showing the Shirase ice tongue. Overlain are
selected ice-front positions from 1963, 1974, 1988, 2000 and 2020; along with the transect, T1, used
to extract ice speed profiles and point x, which is the location of the 1973/74 ice speed estimate on
the floating tongue. Point IT is the location of the ice thickness time-series. The grey line is the
MODIS 2009 grounding line (Scambos et al., 2007, Harran et al., 2021). The coordinate grid is in

182   km. **b)** Change in ice-front extent relative to 1963. **c)** Surface elevation profiles along a small section
183   of T1 as it intersects the grounding line from February 2008, January 2013 and October 2015 showing
184   a seaward migration of the surface slope d) The rift used to estimate ice speed in 1973/74. The red
185   line is the digitized rift from January 1973. **e)** Ice speed profiles from transect T1 between 1973 and
186   2020. The black cross represents the ice speed measurement from 1973/74. Landsat images are
187   courtesy of the U.S. Geological Survey.

189   Ice speed profiles along the transect (T1, Fig. 2a) show a uniform pattern of change across both the
190   grounded and floating sections of Shirase Glacier (Fig. 2e). At the grounding line, we observe little
191   change in ice speed between 1973 and 1988, although we note the larger uncertainty in the 1988
192   estimate of ±171 m a^{-1} (Fig. 3b). Between 1988 and 1996 we observe a 2 $\pm7\%$ slowdown and a 2 $\pm1\%$
193   increase in ice speed between 1997 and 2000 (Fig. 3a). Post-2000 we observe a slowdown, with an 8
194   $\pm1\%$ decrease in ice speed between 2000 and 2015 (Fig. 3b). Between 2015 and 2019 ice speed
195   increased by 4 $\pm1\%$ (Fig. 3a). Elevation profiles along a section of T1 in 2008, 2013 and 2015 show
196   a seaward migration of the surface slope as it approaches the grounding line (Fig. 2d), which is
197   indicative of grounding line advance and can be visualised in animation S3. Between February 2008
198   and October 2015 we estimate that the grounding line has advanced around 400 m (~50 m yr^{-1}) from
199   measuring the seaward displacement of the surface slope, an estimate that is consistent with CryoSat
200   based observations of seaward grounding line migration between 2010 and 2016 (~30 m a^{-1}; Konrad
201   et al., 2018). Observations of ice thickness change 20 km inland of the grounding line show a thinning
202   trend of 0.27 ±0.33 m a^{-1} between 1987 and 1997, before reversing to a thickening trend of 0.19 ±0.10
203   m a^{-1} between 1997 and 2017 (Fig. 3b).

204   ERA5 derived estimates of alongshore wind speed between 1979 and 2020 show limited variation
205   between 1984 and the early 1990s (Fig. 3a). In the early 1990s there was a small increase in
206   alongshore wind speed, before a much more marked increase from 2000-2010 where alongshore wind
207   speed increased from around 4 m s^{-1} to 4.8 m s^{-1} (Fig. 3a). This is before falling slightly to around 4.5
208   m s^{-1} between 2010 and 2018, which is coincident with an increase in basal melt rate anomalies (Fig.
209   3a). Long-term increased alongshore wind speeds at the Syowa research station in Lützow-Holm Bay
210   between 1966 and 2020 are also observed with a small peak in alongshore wind speeds in the early
211   1990s before a sharp increase in along shore wind speed between the late 1990s and 2005 (Fig. S2).
212   However, the observational record at Syowa also records a peak in alongshore wind speed in the early
213   1980s (Fig. S2) that is not present in the ERA5 offshore reanalysis record (Fig. 3a).

214

215
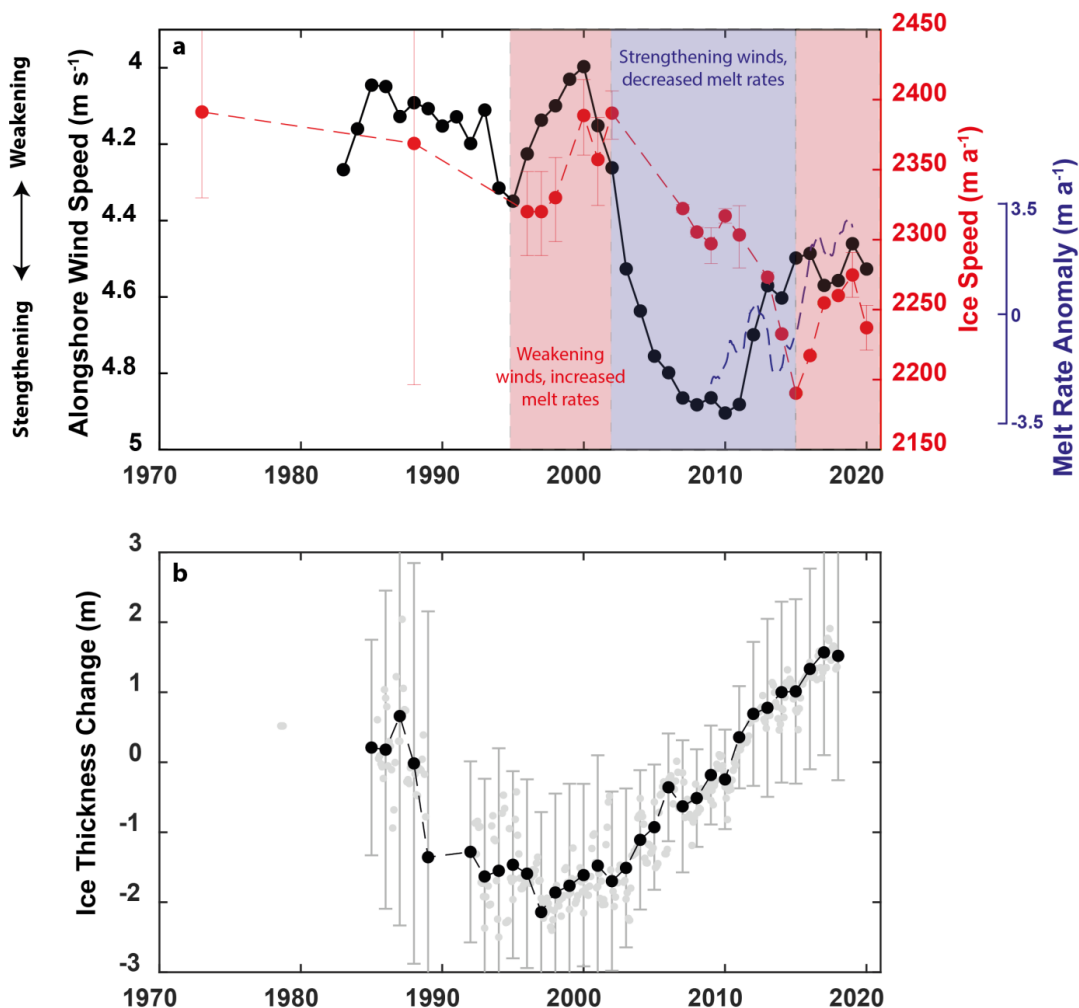
Figure 3: a) Annually averaged ERA5 derived alongshore wind speed from Box A (See Fig. 1) and
plotted as a 5-year rolling mean (black), ice speed at the Shirase Glacier grounding line along T1
(red) and modelled melt rate anomaly of the Shirase ice tongue between 2008 and 2018 (blue;
Kusahara et al., 2021). Periods of weakening winds cause increased mCDW transport, increased basal
melt and acceleration. Periods of strengthening winds result in relatively less mCDW transport,
decreased basal melt rates and glacier slowdown. Note that alongshore wind seed is plotted with an
inverted axis. **b)** Annually averaged ice thickness change at point IT (see Fig. 2a) extracted from the
Schröder et al. (2019) dataset, where there are at least 6 data points in the calendar year. The error
bars are annually averaged errors. The background grey points are the raw monthly data points.

225

226   **4. Discussion**

227   **4.1 Slowdown and thickening caused by strengthening alongshore winds**

228   Theoretical considerations indicate that the heavily fractured and unconstrained section of the Shirase

229   ice tongue offers little buttressing force (Fürst et al., 2016). Therefore, it is unlikely that any varations

230   in the extent of the Shirase ice tongue have had a direct effect on the ice speed trends we have

231   observed (Fig. 4a). The only exception to this is in 1988 where the ice tongue briefly retreated to the

232   edge of its more confined embayment (Fig. 2a), closer to where the extent of the ice tongue might be

233   expected to exert buttressing and impact on inland flow speed, were it to be removed (Fig. 4a).

234
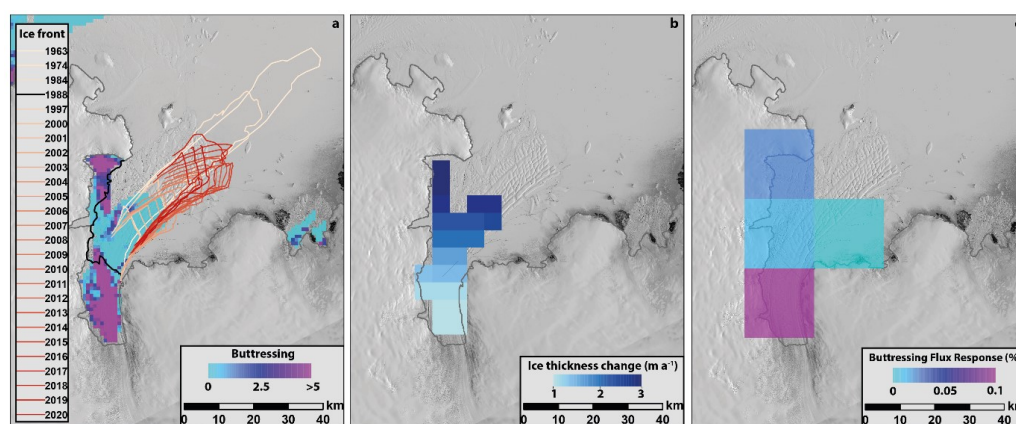
235

236   **Figure 4:** No change in ice tongue buttressing in response to observed changes in ice tongue extent,
237   but increased buttressing expected in response to observed ice tongue thickening. **a)** Simulated
238   maximum buttressing potential of the Shirase ice tongue (Durand et al., 2016). Light blues mean the
239   ice is passive, purples mean the floating ice is dynamically important. No dynamically important ice
240   has calved over the past over the past 57 years. **b)** Ice tongue thickness change between 2003 and
241   2019 showing thickening of the Shirase ice tongue (Smith et al., 2020). **c)** Simulated response of ice
242   flux to thinning of floating ice in each grid cell by 1 m (Reese et al., 2018), floating ice near the
243   grounding line is important for buttressing.

244

245   In agreement with previous work, we note that the observed fluctuations in ice tongue extent are

246   correlated with landfast sea-ice conditions in Lützow-Holm Bay (Aoki, 2017). Long periods of ice

247   tongue advance are associated with persistent landfast sea-ice in Lützow-Holm Bay, while ice tongue

248   retreat is associated with landfast sea-ice break-out events removing parts of the ice tongue

249   conglomerate (Aoki et al., 2017). It is unlikely that the fast ice has any major role in providing

250   buttressing for Shirase Glacier. We note that there was no obvious spike in ice speeds on the

251   grounding line or ice tongue in 1988 when the fast ice was completely removed from the bay (Fig.

252   2a, S3) and that Nakamura et al. (2010) recorded only a very modest 20 ± 30 m a^{-1} (0.8 ± 1.3 %)

253   change in ice speed at the grounding line after a partial fast ice break-out event in 1998.

254   Point IT, 20 km inland of the Shirase Glacier grounding line was thinning at a rate of -0.27 ±0.33 m

255   a^{-1} between 1987 and 1997 (Fig. 3c), a pattern consistent with field observations up to 200 km further

256   inland in the 1960s, 1970s and 1980s (Mae and Naruse, 1978; Naruse, 1979; Nisho et al., 1989; Toh

257   and Shibuya, 1992). However, at ~2000 there was a slowdown in Shirase Glacier (Fig. 3a) and this

258   thinning trend reversed to thickening (Fig. 3b). This slowdown and thickening coincides with an

259   increase in alongshore wind speed adjacent to the Shirase coastline (Fig. 3a). The seasonal

260   strenghtening in alongshore winds offshore of the Shirase coastline has been observed to deepen the

261   thermocline in Lützow-Holm Bay, limiting the inflow of mCDW onto the continental shelf and reduce

262   basal melt rates (Hirano et al., 2020). We suggest that this same process over annual to decadal

263   timescales has caused the slowdown of Shirase Glacier.

264   Increased alongshore wind speed from ~2000 enhanced Ekman convergence at the coast, deepening

265   the thermocline with a short lag and inhibited the inflow of warm mCDW into Lützow-Holm Bay.

266   The subsequent cooling of Lützow-Holm Bay reduced the basal melt rate of the Shirase ice tongue.

267   This reduction in basal melt caused the ice tongue to dynamically thicken and is confirmed by ICESat

268   and ICESat-2 observations of the of the Shirase ice tongue that show a mean thickening of 1.87 m yr^{-}

269   ^{1} from 2003-2019 (Fig. 4b; Smith et al., 2020). The dynamic thickening of the ice tongue increases

270   buttressing through time (Reese et al., 2018; Fig. 4c) and ultimately drives the overall slowdown in

271   ice speed, grounding line advance and inland thickening that we observe. Importantly, our results

272   show that wind-driven ocean forcing is also contributing to the mass gain in the Dronning Maud Land

273   regions in addition to surface mass balance processes (Boening et al., 2012; Lenaerts et al., 2013).

274   Within the longer term slowdown of Shirase Glacier between 1973 and 2020 we observe brief periods

275   of acceleration in response to short-lived periods of weakening alongshore winds. For example, both

276   of the accelerations in ice speed from 1997-2000 and 2015-2019 are preceded by brief periods of

277   weakening alongshore winds (Fig. 3a). These periods of weakening alongshore winds cause relatively

278   higher basal melt rates because they raise the thermocline closer to the ocean surface and enable a

279   greater influx of mCDW into Lützow-Holm Bay (Hirano et al., 2020). For 2015-2019, this is

280   supported by increasingly higher modelled melt rate anomalies (Fig. 3a). Because we observe

281   coincidental acceleration in ice speed during this period of increased melt rates, it is indicative of a

282   reduction in buttressing in response to ice tongue thinning. The interannual variability in ice flow

283   speed at Shirase Glacier in response to wind-forced ocean variability is analogous to other regions of

284   Antarctica where mCDW periodically floods the continental shelf e.g. Pine Island (Christianson et

285   al., 2016), Thwaites (Miles et al., 2020) and Totten Glaciers (Greene et al., 2017). Although, the

286   pattern of change at Shirase Glacier is unique because it is the only outlet glacier in Antarctica with

287   a warm water regime, that has been observed to be slowing down and thickening during the 21st

288   century, as opposed to accelerating and thinning (e.g. Mouginot et al., 2014; Greene et al., 2017).

289   Therefore, this result highlights that this oceanic mode of ice melt is not universally associated with

290   mass loss in Antarctica.

291

292   **4.2 Wider links to climate forcing and future implications**

293   In response to both increased greenhouse gas emissions and ozone depletion (Thompson et al., 2011;

294   Wang et al., 2014; Perren et al., 2020) the band of mid-latitude westerly winds that encircle Antarctica

295   have both strengthened and migrated southwards towards the ice sheet over recent decades

296   (Thompson & Solomon, 2002; Marshall, 2003; Turner, 2005; Bracegirdle et al., 2018). In the

297   Amundsen Sea sector this anthropogenic driven migration has been linked to westerly wind anomalies

298   over the continental shelf (Holland et al., 2019), which have enabled a greater influx of warm mCDW

299   onto the continental shelf and have driven enhanced localized ice sheet mass loss (Thoma et al., 2008).

300   At Shirase Glacier, our observations of strengthening alongshore easterly winds suggest any

301   southward encroachment of the mid-latitude westerlies has yet to impact the Shirase coastline. This

302   may also be the case for parts of the wider Dronning Maud Land coastlines where alongshore

303   easterlies have also been observed to have strengthened (Hazel & Stewart, 2019). This trend in

304   strengthening alongshore easterlies is linked to enhanced katabatic winds as low pressure systems

305   track progressively further south and enhance the pole to coast pressure gradient (Hazel & Stewart,

306   2019). It remains undetermined if the enhancement of the pole to coast pressure gradient has been

307   influenced by the anthropogenically driven southerly migration of the mid-latitude westerlies, or if it

308   has been caused by inherent natural decadal variability within the system.

309   Over the course of the 21st century, the southerly migration of the mid-latitude westerlies is projected

310   to continue in line with a warming climate (Yin, 2005; Perren et al., 2020). Along the Shirase

311   coastline, it remains unclear if this continued southerly migration will ultimately result in a similar

312   situation to the Amundsen Sea, such that westerly wind anomalies offshore would result in enhanced

313   mCDW transport into Lützow-Holm Bay and cause mass loss. Alternatively, the westerly winds may

314   never migrate close enough to the Shirase coastline to impact alongshore winds, and instead,

315   alongshore winds may continue to strengthen as the pole to coast pressure gradient increases. This

316   would result in further cooling of Lützow-Holm Bay and ice tongue thickening, and further mass

317   gain. In a wider context a greater understanding of the potential changes in ocean forcing in response

318   to broader atmospheric patterns expected over the coming decades is needed in the Dronning Maud

319   Land sector.

320

5. Conclusion

Our observations of Shirase Glacier are a rare example of a glacier reversing a trend of mass loss from at least the 1970s-1990s to mass gain over the last two decades. As far as we are aware this is the only major fast flowing Antarctic outler glacier to display this pattern of behaviour. This reversal has been driven by a slowdown of the Shirase Glacier upstream of the grounding line in response to strengthening alongshore winds that have limited the inflow of warm mCDW into Lützow-Holm Bay, reduced basal melt rates and caused its ice tongue to dynamically thicken. This means that ocean forcing has contributed to some of the observed mass gain in Dronning Maud Land. It is not certain if these strengthening alongshore winds represent some form of inherent decadal-scale variability or if they are part of a multi-decadal trend, but we hypothesise that they are at least consistent with an anthropogenically-driven poleward migration of the mid-latitude westerly winds. Should this strengthening of alongshore easterly winds continue into the future, the Shirase catchment will continue to experience a positive mass balance due to both the slow-down in ice discharge, and to the predicted increase in precipitation in response to atmopsheric warming (e.g. Ligtenberg et al., 2013; Kittel et al., 2021). Our results highlight the need for a greater consideration in the potential role of ocean forcing in both the current and future mass balance of the wider Dronning Maud Land region.

Data Availability

Landsat and ARGON imagery was provided free of charge by the US Geological Survey Earth Resources Observation Science Center (https://earthexplorer.usgs.gov/). For the MODIS imagery we also acknowledge the use of imagery from the NASA Worldview application (https://worldview.earthdata.nasa.gov), part of the NASA Earth Observing System Data and Information System (EOSDIS). Cosi-corr is an ENVI plug-in and can be downloaded from http://www.tectonics.caltech.edu/slip_history/spot_coseis/download_software.html. The ITS_LIVE velocity products are available from https://doi.org/10.5067/IMR9D3PEI28U. GoLIVE velocity products are avaialble from http://dx.doi.org/10.7265/N5ZP442B. ERA5 data is available from https://doi.org/10.24381/cds.adbb2d47. Wind data from Syowa station is available via the SCAR READER at http://dx.doi.org/10.5285/569d53fb-9b90-47a6-b3ca-26306e696706. The MOA grounding line product is avaialble at https://doi.org/10.7265/N5KP8037. BedMachine is available at https://doi.org/10.5067/E1QL9HFQ7A8M. The ice shelf thickness change dataset from Smith et al. (2020) is available at http://hdl.handle.net/1773/45388. REMA DEM strips are avialble at https://www.pgc.umn.edu/data/rema/. Lützow-Holm Bay bathymetry is available at

354   https://doi.org/10.17632/z6w4xd6s3s.1. The RAMP mosaic is available at https://doi.org/10.5

355   067/8AF4ZRPULS4H. Ice shelf extent buttressing dataset from Durand et al., 2016 is available at

356   https://doi.org/10.5067/FWHORAYVZCE7.   SPIRIT   DEM's   are   available   from

357   https://theia.cnes.fr/atdistrib/rocket/#/search?collection=Spirit

358

359   **Acknowledgements**

360   This research has been supported by a UK Natural Environment Research Council (NERC) grant
361   (NE/R000824/1). BM was also supported by a Leverhulme Early Career Fellowship (ECF-2021-
362   484). Hersbach, H. et al.'s (2018) dataset was downloaded from the Copernicus Climate Change
363   Service (C3S) Climate Data Store. We acknowledge the DEMs provided by the Byrd Polar and
364   Climate Research Center and the Polar Geospatial Center under NSF-OPP awards 1543501, 1810976,
365   1542736, 1559691, 1043681, 1541332, 0753663, 1548562, 1238993 and NASA award
366   NNX10AN61G. Computer time provided through a Blue Waters Innovation Initiative. DEMs
367   produced using data from Maxar. We thank Ronja Reese for providing the ice flux buttressing
368   response dataset.

369

370   **Author contributions:** All authors contributed to the design of the study. BWJM collected and

371   analysed the remote sensing data and led the manuscript writing with input from all authors.

372

373   **Competing interests:** The authors declare no competing interests

374

375

376

377

378

379

380

381

382

383

384

385 **References**

386 Aoki, S., Ozawa, T. & Doi, K. (2000). GPS observation of the sea level variation in Lützow-Holm
387   Bay, Antarctica. *Geophysical Research Letters, 27(15), 2285-2288.*
388   *https://doi.org/10.1029/1999GL011304*

389 Aoki, S. (2017). Breakup of land-fast sea ice in Lützow-Holm Bay, East Antarctica, and its
390   teleconnection to tropical Pacific sea surface temperatures. *Geophysical Research Letters*,
391   *44*(7), 3219–3227. https://doi.org/10.1002/2017GL072835

392 Aoyama, Y., Doi, K., Shibuya, K., Ohta, H., & Tsuwa, I. (2013). Near real-time monitoring of flow
393   velocity and direction in the floating ice tongue of the Shirase Glacier using low-cost GPS
394   buoys. *Earth, Planets and Space*, *65*(2), 103–108. https://doi.org/10.5047/EPS.2012.06.011

395 Boening, C., Lebsock, M., Landerer, F., & Stephens, G. (2012). Snowfall-driven mass change on
396   the East Antarctic ice sheet. *Geophysical Research Letters*, *39*(21).
397   https://doi.org/10.1029/2012GL053316

398 Bracegirdle, T. J., Hyder, P., & Holmes, C. R. (2018). CMIP5 Diversity in Southern Westerly Jet
399   Projections Related to Historical Sea Ice Area: Strong Link to Strengthening and Weak Link to
400   Shift. *Journal of Climate*, *31*(1), 195–211. https://doi.org/10.1175/JCLI-D-17-0320.1

401 Brunt, K. M., Fricker, H. A., Padman, L., Scambos, T. A., & O'Neel, S. (2010). Mapping the
402   grounding zone of the Ross Ice Shelf, Antarctica, using ICESat laser altimetry. Annals of
403   Glaciology, 51(55), 71–79. https://doi.org/10.3189/172756410791392790

404 Christianson, K., Bushuk, M., Dutrieux, P., Parizek, B. R., Joughin, I. R., Alley, R. B., et al. (2016).
405   Sensitivity of Pine Island Glacier to observed ocean forcing. *Geophysical Research Letters*,
406   *43*(20), 10,817-10,825. https://doi.org/10.1002/2016GL070500

407 Cook, A. J., Holland, P. R., Meredith, M. P., Murray, T., Luckman, A., & Vaughan, D. G. (2016).
408   Ocean forcing of glacier retreat in the western Antarctic Peninsula. *Science*, *353*(6296), 283–
409   286.

410 Durand, G., F. Gillet-Chaulet, O. Gagliardini, and J. J. Fürst. (2016). SUMER Antarctic Ice-shelf
411   Buttressing, Version 1. Boulder, Colorado USA. NASA National Snow and Ice Data Center
412   Distributed Active Archive Center. https://doi.org/10.5067/FWHORAYVZCE7.

413 Fahnestock, M., Scambos, T., Moon, T., Gardner, A., Haran, T., & Klinger, M. (2016). Rapid large-
414   area mapping of ice flow using Landsat 8. *Remote Sensing of Environment*, *185*, 84–94.
415   https://doi.org/10.1016/J.RSE.2015.11.023

416 Fricker, H. A., Coleman, R., Padman, L., Scambos, T. A., Bohlander, J., & Brunt, K. M. (2009).
417   Mapping the grounding zone of the Amery Ice Shelf, East Antarctica using InSAR, MODIS
418   and ICESat. Antarctic Science, 21(5), 515–532. https://doi.org/10.1017/S095410200999023X

419 Fürst, J. J., Durand, G., Gillet-Chaulet, F., Tavard, L., Rankl, M., Braun, M., & Gagliardini, O.
420   (2016). The safety band of Antarctic ice shelves. *Nature Climate Change*, *6*(5), 479–482.
421   https://doi.org/10.1038/nclimate2912

422 Gardner, A., Fahnestock, M., & Scambos, T. A. (2020). ITS_LIVE Regional Glacier and Ice Sheet
423   Surface Velocities. https://doi.org/doi:10.5067/6II6VW8LLWJ7

424 Gardner, A. S., Moholdt, G., Scambos, T., Fahnstock, M., Ligtenberg, S., van den Broeke M., &
425   Nilsson, J. (2018). Increased West Antarctic and unchanged East Antarctic ice discharge over
426   the last 7 years. *Cryosphere*, *12*(2), 521–547. https://doi.org/10.5194/TC-12-521-2018

427 Greene, C. A., Blankenship, D. D., Gwyther, D. E., Silvano, A., & van Wijk, E. (2017). Wind
428   causes Totten Ice Shelf melt and acceleration. *Science Advances*, *3*(11), e1701681–e1701681.
429   https://doi.org/10.1126/sciadv.1701681

430 Haran, T., J. Bohlander, T. Scambos, T. Painter, and M. Fahnestock. (2019), updated 2019. MODIS
431   Mosaic of Antarctica 2008-2009 (MOA2009) Image Map, Version 2. Boulder, Colorado USA.
432   NASA National Snow and Ice Data Center Distributed Active Archive Center. doi:
433   https://doi.org/10.5067/4ZL43A4619AF.

434 Hazel, J. E., & Stewart, A. L. (2019). Are the Near-Antarctic Easterly Winds Weakening in
435   Response to Enhancement of the Southern Annular Mode? *Source: Journal of Climate*, *32*(6),
436   1895–1918. https://doi.org/10.2307/26663209

437 Hersbach, H., Bell, B., Berrisford, P., Hirahara, S., Horányi, A., Muñoz-Sabater, J., et al. (2020).
438   The ERA5 global reanalysis. *Quarterly Journal of the Royal Meteorological Society*, *146*(730),
439   1999–2049. https://doi.org/10.1002/QJ.3803

440 Heid, T., & Kääb, A. (2012). Evaluation of existing image matching methods for deriving glacier
441   surface displacements globally from optical satellite imagery. Remote Sensing of
442   Environment, 118, 339–355. https://doi.org/10.1016/J.RSE.2011.11.024

443 Hirano, D., Tamura, T., Kusahara, K., Ohshima, K. I., Nicholls, K. W., Ushio, S., et al. (2020).
444   Strong ice-ocean interaction beneath Shirase Glacier Tongue in East Antarctica. *Nature
445   Communications 2020 11:1*, *11*(1), 1–12. https://doi.org/10.1038/s41467-020-17527-4

446 Holland, P. R., Bracegirdle, T. J., Dutrieux, P., Jenkins, A., & Steig, E. J. (2019). West Antarctic ice
447   loss influenced by internal climate variability and anthropogenic forcing. *Nature Geoscience
448   2019 12:9*, *12*(9), 718–724. https://doi.org/10.1038/s41561-019-0420-9

449 Howat, I. M., Porter, C., Smith, B. E., Noh, M. J., & Morin, P. (2019). The reference elevation
450   model of antarctica. Cryosphere, 13(2), 665–674. https://doi.org/10.5194/TC-13-665-2019

451 Jacobs, S. S., Helmer, H. H., Doake, C. S. M., Jenkins, A., & Frolich, R. M. (1992). Melting of ice
452   shelves and the mass balance of Antarctica. *Journal of Glaciology*, *38*(130), 375–387.
453   https://doi.org/10.3189/S0022143000002252

454 Jenkins, A., Shoosmith, D., Dutrieux, P., Jacobs, S., Kim, T. W., Lee, S. H., et al. (2018). West
455   Antarctic Ice Sheet retreat in the Amundsen Sea driven by decadal oceanic variability, *11*(10),
456   733–738. https://doi.org/10.1038/s41561-018-0207-4

457 Jezek, K. C., J. C. Curlander, F. Carsey, C. Wales, and R. G. Barry. (2013). RAMP AMM-1 SAR
458   Image Mosaic of Antarctica, Version 2. Boulder, Colorado USA. NASA National Snow and
459   Ice Data Center Distributed Active Archive Center. https://doi.org/10.5067/8AF4ZRPULS4H.

460 Kameda, T., Nakawo, M., Mae, S., Watanabe, O., & Naruse, R. (1990). Thinning of the Ice Sheet
461   Estimated from Total Gas Content of Ice Cores in Mizuho Plateau, East Antarctica. *Annals of
462   Glaciology*, *14*, 131–135. https://doi.org/10.3189/S0260305500008429

Kittel, C., Amory, C., Agosta, C., Jourdain, N. C., Hofer, S., Delhasse, A., et al. (2021). Diverging future surface mass balance between the Antarctic ice shelves and grounded ice sheet. *Cryosphere*, *15*(3), 1215–1236. https://doi.org/10.5194/TC-15-1215-2021

Konrad, H., Shepherd, A., Gilbert, L., Hogg, A. E., McMillan, M., Muir, A., & Slater, T. (2018). Net retreat of Antarctic glacier grounding lines. Nature Geoscience, 11(4), 258–262. https://doi.org/10.1038/s41561-018-0082-z

Korona, J, Berthier, E, Bernard, M, Rémy, F and Thouvenot, E (2009) ISPRS Journal of Photogrammetry and Remote Sensing SPIRIT. SPOT 5 stereoscopic survey of Polar Ice: reference images and topographies during the fourth International Polar Year (2007–2009). ISPRS Journal of Photogrammetry and Remote Sensing 64(2), 204–212. doi: 10.1016/j.isprsjprs.2008.10.005.

Kusahara, K., Hirano, D., Fujii, M., D. Fraser, A., & Tamura, T. (2021). Modeling intensive ocean-cryosphere interactions in Lützow-Holm Bay, East Antarctica. *Cryosphere*, *15*(4), 1697–1717. https://doi.org/10.5194/TC-15-1697-2021

Lenaerts, J. T. M., van Meijgaard, E., van den Broeke, M. R., Ligtenberg, S. R. M., Horwath, M., & Isaksson, E. (2013). Recent snowfall anomalies in Dronning Maud Land, East Antarctica, in a historical and future climate perspective. *Geophysical Research Letters*, *40*(11), 2684–2688. https://doi.org/10.1002/GRL.50559

Leprince, S., Ayoub, F., Klinger, Y., & Avouac, J.-P. (2007). *Co-Registration of Optically Sensed Images and Correlation (COSI-Corr): an Operational Methodology for Ground Deformation Measurements*. Igarss: 2007 Ieee International Geoscience and Remote Sensing Symposium, 1–12,1943–1946. https://doi.org/10.1109/Igarss.2007.4423207

Ligtenberg, S. R. M., van de Berg, W. J., van den Broeke, M. R., Rae, J. G. L., & van Meijgaard, E. (2013). Future surface mass balance of the Antarctic ice sheet and its influence on sea level change, simulated by a regional atmospheric climate model. *Climate Dynamics*, *41*(3–4), 867–884. https://doi.org/10.1007/S00382-013-1749-1

Mae, S., & Naruse, R. (1978). Possible causes of ice sheet thinning in the Mizuho Plateau. *Nature 1978 273:5660*, *273*(5660), 291–292. https://doi.org/10.1038/273291a0

Marshall, G. (2003). Trends in the Southern Annular Mode from observations and reanalyses. *J. Clim.*, *16*, 4134–4143.

Miles, B. W. J. J., Stokes, C. R., Jenkins, A., Jordan, J. R., Jamieson, S. S. R. R., & Gudmundsson, G. H. (2020). Intermittent structural weakening and acceleration of the Thwaites Glacier Tongue between 2000 and 2018. *Journal of Glaciology*, 1–11. https://doi.org/10.1017/jog.2020.20

Moriwaki, K., & Yoshida, Y. (1983). Submarine topography of Lützow-Holm Bay, Antarctica. *Mem. Natl. Inst. Polar Res.*, *28*, 247–258.

Morlighem, M. (2020). MEaSUREs BedMachine Antarctica, Version 2. Boulder, Colorado USA. NASA National Snow and Ice Data Center Distributed Active Archive Center. doi: https://doi.org/10.5067/E1QL9HFQ7A8M.

Morlighem, M., Rignot, E., Binder, T., Blankenship, D., Drews, R., Eagles, G., et al. (2020). Deep glacial troughs and stabilizing ridges unveiled beneath the margins of the Antarctic ice sheet. *Nature Geoscience*, *13*(2), 132–137. https://doi.org/10.1038/s41561-019-0510-8

505 Mouginot, J., Rignot, E., & Scheuchl, B. (2014). Sustained increase in ice discharge from the
506   Amundsen Sea Embayment, West Antarctica, from 1973 to 2013. *Geophysical Research*
507   *Letters*, *41*(5), 1576–1584. https://doi.org/10.1002/2013GL059069

508 Nakamura, K., Doi, K., & Shibuya, K. (2007). Estimation of seasonal changes in the flow of
509   Shirase Glacier using JERS-1/SAR image correlation. *Polar Science*, *1*(2–4), 73–83.
510   https://doi.org/10.1016/J.POLAR.2007.09.002

511 Nakamura, K., Doi, K., & Shibuya, K. (2010). Fluctuations in the flow velocity of the Antarctic
512   Shirase Glacier over an 11-year period. *Polar Science*, *4*(3), 443–455.
513   https://doi.org/10.1016/J.POLAR.2010.04.010

514 Naruse, R. (1979). Thinning of the Ice Sheet in Mizuho Plateau, East Antarctica. *Journal of*
515   *Glaciology*, *24*(90), 45–52. https://doi.org/10.3189/S0022143000014635

516 Nishio, F., Mae, S., Ohmae, H., Takahashi, S., Nakawo, M., & Kawada, K. (1989). Dynamical
517   behaviour of the ice sheet in Mizuho Plateau, East Antarctica. *Proc. NIPR Symp. Polar*
518   *Meteorol. Glaciol.*, *2*, 97–104.

519 Ohshima, K. I., Takizawa, T., Ushio, S., & Kawamura, T. (1996). Seasonal variations of the
520   Antarctic coastal ocean in the vicinity of Lützow-Holm Bay. *Journal of Geophysical Research*
521   *C: Oceans*, *101*(C9), 20617–20628. https://doi.org/10.1029/96JC01752

522 Pattyn, F., & Derauw, D. (2002). Ice-dynamic conditions of Shirase Glacier, Antarctica, inferred
523   from ERS SAR interferometry. *Journal of Glaciology*, *48*(163), 559–565.
524   https://doi.org/10.3189/172756502781831115

525 Pattyn, F., & Naruse, R. (2003). The nature of complex ice flow in Shirase Glacier catchment, East
526   Antarctica. *Journal of Glaciology*, *49*(166), 429–436.
527   https://doi.org/10.3189/172756503781830610

528 Perren, B. B., Hodgson, D. A., Roberts, S. J., Sime, L., van Nieuwenhuyze, W., Verleyen, E., &
529   Vyverman, W. (2020). Southward migration of the Southern Hemisphere westerly winds
530   corresponds with warming climate over centennial timescales. *Communications Earth &*
531   *Environment 2020 1:1*, *1*(1), 1–8. https://doi.org/10.1038/s43247-020-00059-6

532 Reese, R., Gudmundsson, G. H., Levermann, A., & Winkelmann, R. (2018). The far reach of ice-
533   shelf thinning in Antarctica. Nature Climate Change, 8(1), 53– 57.
534   https://doi.org/10.1038/s41558-017-0020-x

535 Rignot, E., Mouginot, J., Scheuchl, B., van den Broeke, M., van Wessem, M. J., & Morlighem, M.
536   (2019, January 22). Four decades of Antarctic ice sheet mass balance from 1979–2017.
537   *Proceedings of the National Academy of Sciences of the United States of America*. National
538   Academy of Sciences. https://doi.org/10.1073/pnas.1812883116

539 Rintoul, S. R., Silvano, A., Pena-Molino, B., van Wijk, E., Rosenberg, M., Greenbaum, J. S., &
540   Blankenship, D. D. (2016). Ocean heat drives rapid basal melt of the Totten ice shelf. *Science*
541   *Advances*, *2*(12). https://doi.org/10.1126/sciadv.1601610

542 Scambos, T., Fahnestock, M., Moon, T., Gardner, A., & Klinger, M. (2016). Global Land Ice
543   Velocity Extraction from Landsat 8 (GoLIVE). Boulder, Colorado USA. NSIDC: National
544   Snow and Ice Data Center.

545   Scambos, T. A., Haran, T. M., Fahnestock, M. A., Painter, T. H., & Bohlander, J. (2007). MODIS-
546   based Mosaic of Antarctica (MOA) data sets: Continent-wide surface morphology and snow
547   grain size. *Remote Sensing of Environment*, *111*(2), 242–257.
548   https://doi.org/10.1016/J.RSE.2006.12.020

549   Scherler, D., Leprince, S., & Strecker, M. R. (2008). Glacier-surface velocities in alpine terrain
550   from optical satellite imagery—Accuracy improvement and quality assessment. *Remote*
551   *Sensing of Environment*, *112*(10), 3806–3819. https://doi.org/10.1016/J.RSE.2008.05.018

552   Schröder, L., Horwath, M., Dietrich, R., & Helm, V. (2019). Four decades of surface elevation
553   change of the Antarctic Ice Sheet from multi-mission satellite altimetry. *The Cryosphere*, 13,
554   427–449, https://doi.org/10.5194/tc-13-427-2019

555   Smith, B., Fricker, H. A., Gardner, A. S., Medley, B., Nilsson, J., Paolo, F. S., Nicholas Holschuh,
556   et al. (2020). Pervasive ice sheet mass loss reflects competing ocean and atmosphere processes.
557   *Science*, *368*(6496), 1239–1242.

558   Sproson, A. D., Takano, Y., Miyairi, Y., Aze, T., Matsuzaki, H., Ohkouchi, N., & Yokoyama, Y.
559   (2021). Beryllium isotopes in sediments from Lake Maruwan Oike and Lake Skallen, East
560   Antarctica, reveal substantial glacial discharge during the late Holocene. *Quaternary Science*
561   *Reviews*, *256*, 106841. https://doi.org/10.1016/J.QUASCIREV.2021.106841

562   Thoma, M., Jenkins, A., Holland, D., & Jacobs, S. (2008). Modelling Circumpolar Deep Water
563   intrusions on the Amundsen Sea continental shelf, Antarctica. *Geophysical Research Letters*,
564   *35*(18). https://doi.org/10.1029/2008GL034939

565   Thompson, D. W. J., & Solomon, S. (2002). Interpretation of recent Southern Hemisphere climate
566   change. *Science*, *296*(5569), 895–899. https://doi.org/10.1126/science.1069270

567   Thompson, D. W. J., Solomon, S., Kushner, P. J., England, M. H., Grise, K. M., & Karoly, D. J.
568   (2011). Signatures of the Antarctic ozone hole in Southern Hemisphere surface climate change.
569   *Nature Geoscience 2011 4:11*, *4*(11), 741–749. https://doi.org/10.1038/ngeo1296

570   Toh, H. and Shibuya, K. (1992). Thinning rate of ice sheet on Mizuho Plateau, East Antarctica,
571   determined by GPS differential positioning. In Yoshida, Y., Kaminuma, K. and Shiraishi, K.,
572   eds. Recent progress in Antarctic earth sciences. Tokyo, Terra Scientific Publishing Co., 579–
573   583.

574   Turner, J., Colwell, S. R., Marshall, G. J., Lachlan-Cope, T. A., Carleton, A. M., Jones, P. D.,
575   Lagun, V., Reid, P. A., & Iagovkina, S. (2004). The SCAR READER Project: Toward a High-
576   Quality Database of Mean Antarctic Meteorological Observations, Journal of Climate, 17(14),
577   2890-2898.

578   Turner, J. (2005). Antarctic climate change during the last 50 years. *Int. J. Climatol.*, *25*, 279–294.

579   Wang, G., Cai, W., & Purich, A. (2014). Trends in Southern Hemisphere wind-driven circulation in
580   CMIP5 models over the 21st century: Ozone recovery versus greenhouse forcing. *Journal of*
581   *Geophysical Research: Oceans*, *119*(5), 2974–2986. https://doi.org/10.1002/2013JC009589

582   Yin, J. H. (2005). A consistent poleward shift of the storm tracks in simulations of 21st century
583   climate. *Geophys. Res. Lett.*, *32*(18), L18701. https://doi.org/10.1029/2005gl023684

584